Supplement of Atmos. Chem. Phys., 22, 5515–5533, 2022
https://doi.org/10.5194/acp-22-5515-2022-supplement

Atmospheric Chemistry and Physics
Open Access

Supplement of

Offline analysis of the chemical composition and hygroscopicity of submicrometer aerosol at an Asian outflow receptor site and comparison with online measurements

Yange Deng et al.

Correspondence to: Michihiro Mochida (mochida@isee.nagoya-u.ac.jp)

Text S1: Data screening and handling of filter samples

The RH and temperature values were recorded every 5 s during offline experiments using HTDMA. For derivation of the hygroscopic growth factors, only data obtained when the RH values at the outlet of DMA2 during a voltage scan (3 min) were used when they fulfilled the following two criteria: 1) the absolute difference between the mean and setting RH values was less than 0.5 %; 2) the absolute standard deviation of the RH values was less than 0.2 %.

Chemical analyses of OC/EC, WSOC, and ions were performed two or more times for a series of samples. Results from the last series of the analyses for all samples were regarded as the most reliable and were used for this study. As described in our earlier report, sampling of $PM_{0.95}$ on 8 × 10 inch filters accompanies high loading of aerosol samples at the corners and edges of the effective sampling area (Chen et al., 2017). At least for the last series of quantification using ion chromatograph, carbon analyzer, and TOC analyzer (for WSOC), we specifically devoted attention to avoiding the use of aerosol samples at the corners and edges of the effective sampling area. Positions of the effective sampling area were assumed to be at the center of the filters, although they must have differed slightly from sample to sample. The available record of the positions for TOC analysis is incomplete but there is no indication of the use of punches at edges/corners. Although this non-uniformity was not considered at the time of sample extraction for HTDMA and offline-AMS analyses, good agreement between the calculated atmospheric concentrations of WSOM from the TOC analysis and the OM:OC of WSOM and those from the AMS analysis alone (Text S5, Fig. S6) indicates that bias from non-uniformity, even if it exists, is expected to be slight.

Malfunction of the chopper in the AMS occurred during its online W-mode operation in Okinawa in the period of 28–31 October 2015. The period from the first to the last cases that airbeam correction factor was greater than 1.2 was estimated to be under the influence of the malfunction. The W-mode data during the period were excluded from the analysis. Note that, for both V- and W-modes, effective ambient measurement data were not collected temporarily also in other times during the campaign.

Text S2: Calibration of DMA size selection

Size selection of the two DMAs in the HTDMA for offline analysis was assessed by measuring the number–size distributions of 55, 100, 309, and 498 nm standard size PSL particles (models SC-0055-D, SC-0100-D, and SC-032-S, JSR, and model 3500A, Thermo Fisher Scientific Inc.) followed by determination of their mode diameters by fitting. Whereas the measured mode diameters of 100 and 309 nm PSL particles were within the prescribed expanded uncertainty ranges, the measured mode diameters of 55 and 498 nm PSL particles were greater than the upper ends of the manufacturers' warranties: 10.4 % and 1.91 %, respectively, for 55 and 498 nm particles (Table S2). Differences for 55 and 498 nm are not expected to influence the analyses greatly because the set diameter of DMA1 was 100 nm and because the measured hygroscopic growth factors of the WSM samples were within the range of 0.98–1.88, corresponding to diameters of 98–188 nm. The size selection of SMPS for the online atmospheric measurement was also assessed by measuring the number–size distributions of 55, 100, 309, and 498 nm standard size PSL particles (models are given above). Whereas the measured mode diameters of 55 nm PSL particles were 9.6 % greater than the upper end of the manufacturer's warranty, the measured mode diameters of PSL particles with other sizes were within the ranges of the prescribed expanded uncertainty.

Text S3: Evaluation of HTDMA measurements using AS solution

To evaluate HTDMA performance for hygroscopic growth measurements, the hygroscopic growth of AS particles was measured using the HTDMA following the same procedure as that for WSM particles. Results were compared with those predicted using the E-AIM III model (Text S6, Fig. S3a). Here, the accuracy of RH measurements by Vaisala's sensors is ≤ 2 % according to the manufacturer's warranty. Smaller than expected deliquescence RH (DRH, between 70–75 % versus 80 % (Tang and Munkelwitz, 1994)) and efflorescence RH (ERH, approx. 30 % versus 37 % (Tang and Munkelwitz, 1994)) of AS might be the result of the history of RH in and downstream of NH2, until AS particles were transferred to DMA2 in the HTDMA. The differences provide a guide to uncertainty of the DRH and ERH measurements.

Furthermore, for AS in the humidification branch, except at 20–30 and 85 % RH, and in the dehumidification branch at 30–65 and 90 % RH, great disagreement was observed between measured and predicted κ_{AS} (predicted values deviated from those of measured ones by >15 %, Fig. S3b), which implies some bias of the measured RH and/or of analysis based on the E-AIM model. Because the differences would strongly affect quantitative analysis results if they rely on a combination of measurements and the E-AIM model, only data at 85 % RH in the humidification branch and the RH range of 65–85 % in the dehumidification branch were used to calculate the hygroscopicity parameters for WSOM (κ_{WSOM}) and EOM (κ_{EOM}). Note that the determined values of g_{f} were nearly unity or greater at all RH for both AS (>0.996) and WSM (>0.997) (Fig. S3 and Sect. 3.2). Therefore, there is no indication of non-sphericity of dried particles in the HTDMA (Gysel et al., 2004; Jung et al., 2011).

Text S4: Sample blank evaluation and HTDMA measurement repeatability

Blank filters were extracted using the same procedure as that used for aerosol sample filters (Sect. 2.1). Volume–size distributions of the obtained WSM particles were scanned using SMPS under dry conditions. Results (Fig. S4) show that the volume concentrations of the WSM particles obtained from the blank sample were much lower than those of the aerosol samples. At the dry diameter of 100 nm, the volume concentration of WSM particles from blank samples was, on average, 1.9 % (range 0.9 %–18 %) of those from aerosol samples. These results suggest that possible interference by non-volatile contaminants is, in general, small.

To assess the repeatability of the HTDMA analysis, the hygroscopic growth of WSM particles from sample OKNW_035 was measured three more times in both humidification and dehumidification modes more than five months after measurement of all extracted samples. Both extraction by water and measurement by HTDMA were repeated three times. Results of the additional three measurements are presented in Fig. S5. The standard deviations of g_f in the humidification (or dehumidification) branch were 0.01 (or 0.005), 0.02 (or 0.03), and 0.04 (or 0.02) respectively at 80, 85, and 90 %. The relative standard deviations of the measured g_f were smaller than 6 %, even in the RH range of 60–75 %, where deliquescence of the WSM aerosol particles might have occurred. The values of g_f from first measurements at 80, 85, and 90% RH were larger than the mean of the three repeat measurements in the humidification (or dehumidification) branch by 5.4 (or 3.2), 4.7 (or 5.6), and 3.0 (or 7.3) %, without correction for the slight difference of the sizing (Sect. 2.2) between DMA1 and DMA2. The first measurement was not included in the repeatability analysis because a possible change of the condition of the HTDMA during the long interval might have affected the result.

Text S5: Quantification of WSOM and WISOM based on mass spectra

The mass concentrations of WSOM and WISOM were determined using a phthalic acid method (Han et al., 2016) as follows. The mass spectra of WSOM (or WISOM), pure phthalic acid, and the mixtures of WSOM (or WISOM) and phthalic acid were obtained from offline AMS analysis. The mass ratios of WSOM (or WISOM) to phthalic acid in the mixtures (R_m) were calculated assuming the normalized mass spectra of the mixture are linear combinations of those of WSOM (or WISOM) and pure phthalic acid. For the calculation of R_m, the same relative ionization efficiency was applied for WSOM (or WISOM) and phthalic acid. The signal at m/z 38 was excluded from the analysis for the quantification because it showed negative values and suggests that the contribution of $^{38}Ar^+$ signal was not subtracted in an appropriate quality. The mass concentration of WSOM (or WISOM) (m_{OM}, μg m^{-3}) is calculable using Eq. S1 as shown below.

$$m_{\mathrm{OM}} = \frac{10^6 R_{\mathrm{m}} C_{\mathrm{ph}} M_{\mathrm{ph}} M_{\mathrm{T}} A_{\mathrm{T}}}{100 M_{\mathrm{ext}} A_{\mathrm{ext}} V_{\mathrm{T}}} \tag{S1}$$

Therein, C_{ph} (weight %) represents the mass concentration of phthalic acid in water (or dichloromethane/methanol) solution, M_{ph} (g) is the mass of the phthalic acid solution added to the mixture, M_{ext} (g) is the mass of the WSM (or WISOM) solution added to the mixture, M_{T} (g) is the total mass of the extracted WSM (or WISOM) solution, A_{ext} (cm^2) is the area of the filter used for the extraction, A_{T} (cm^2) is the total filter area subjected to aerosol sample collection, and V_{T} (m^3) is the total volume of air sampled during the aerosol collection. The mass concentration of WSOM derived here shows good agreement with that derived as the product of WSOC from the TOC analyzer and the OM:OC of WSOM (Fig. S6). The consistent result supports the propriety of the quantification of WSOM and WSOC.

Text S6: Hygroscopic growth of WSM predicted using the E-AIM model

Hygroscopic growth of WSM without consideration of water uptake by WSOM and that of ammonium sulfate (AS) particles as a function of water activity (a_{w}) at 0.10 to 0.99, and also the corresponding hygroscopicity parameter (κ) were derived based on the output of the online E-AIM III model and the κ- Köhler theory as described below.

For application of the E-AIM III model to WSM, ammonium, sodium, and sulfate among quantified anions were considered because the concentrations of other ions were low (Table 3). Excess anions in each WSM solution were assumed to be in balance with protons electrically. The a_{w} range of 0.10–0.99 at a resolution of 0.01 was applied to each WSM solution and the AS solution at 298.15 K. In all calculations, the partitioning of HNO_3, HCl, H_2SO_4, and NH_3 to the gas phase was prevented. Furthermore, for the dehumidification branch, the formation of solids was also prevented. The quantity of water as a function of a_{w} in thermodynamically equilibrium conditions was obtained from the model. The hygroscopic growth factor was calculated as the ratio of the sum of the volumes of water and dry WSM (or AS) particle to the volume of dry WSM (or AS) particle. The volumes of dry WSIM and WSOM were calculated in the same manner as that stated in Text S7. The hygroscopicity parameter of WSM (κ_{WSM}), WSIM (κ_{inorg}), and AS (κ_{AS}) was derived following Eq. 2 in Petters and Kreidenweis (2007).

For WSM particles from atmospheric samples, the exponential part of the κ- Köhler equation, which represents the curvature (Kelvin) effect, was calculated on the assumption that the surface tension is that of pure water, the partial molar volume of water in the solution is equal to that of pure water, and that the volumes of WSOM in the particles were considered whereas the water uptake by the WSOM component was ignored. In the case of AS particles, the surface tension of the solution obtained from the E-AIM model was used instead for the calculation. The RH above the particle surface was then calculated as the product of a_w and the corresponding exponential part. The κ_{WSM} and κ_{inorg} (or κ_{AS}) at the measured RH (i.e., 20, 30, 40, 50, 60, 65, 70, 75, 80, 85, and 90 %) were determined by looking up the a_w-κ_{WSM}-κ_{inorg}-RH (or a_w-κ_{AS}-RH) table at a resolution of 0.01.

Text S7: Derivation of volume concentrations of WSIM, WSOM, WISOM, and EC in $PM_{0.95}$

The chemical composition obtained from the offline analysis (Sect. 2.3) was used to derive the volume concentrations of WSIM, WSOM, WISOM, and EC for reconstruction of the hygroscopicity of WSOM, EOM and $PM_{0.95}$. To ascertain the volume concentration of WSIM, the respective contributions from potassium, calcium, magnesium, nitrate, and chloride were ignored because their contributions were minimal compared to those of sulfate, ammonium, and sodium (Table S3). Furthermore, sulfate in the dry condition was assumed to be present preferentially in the form of sodium sulfate (Na_2SO_4). The remaining sulfate was assumed to be present in the form of ammonium sulfate (AS, $(NH_4)_2SO_4$), letovicite (LET, $(NH_4)_3H(SO_4)_2$), ammonium hydrogen sulfate (AHS, NH_4HSO_4), and/or sulfuric acid (SA, H_2SO_4) according to the molar ratios of ammonium to the remaining sulfate ($R_{A/S}$) as follows: ammoniated sulfate was in the form of AS and LET for $1.5<R_{A/S}\leq2$, in the form of LET and AHS for $1<R_{A/S}\leq1.5$, and in the form of SA and AHS for $0<R_{A/S}\leq1$. The volume concentration of WSOM (or WISOM) was found as the ratio of its mass concentration to its density calculated using its O:C and H:C from the offline AMS analysis. The volume concentration of EOM was equal to the sum of the volume concentrations of WSOM and WISOM. The volume concentration of WSM was inferred as the sum of the volume concentrations of WSIM and WSOM. The volume concentration of EC was found using the EC mass concentration from OC/EC analysis, with the assumed density of 1.77 g cm^{-3} (Park et al., 2004).

Text S8: Comparisons between offline and online analyses based on organic mass spectra

Mass spectra of organics at m/z 43, 44, 55, and 57, and the atomic ratios of O to C and H to C are commonly used to characterize the aging and source characteristics of OA. Whereas the comparison between offline and online analyses of O:C is made in Sect. 3.1, here, the mass fractions of m/z 43 (or m/z 44) in organics, f_{43} (or f_{44}), the ratio of the mass fraction of m/z 55 in organics to that of m/z 57 (f_{55}/f_{57}), and H:C between offline and online analyses were compared. The results are presented in Fig. S9. For the days when the mass concentration of organics was high ($m_{OA,online} > 0.2$ μg m^{-3}), the offline and online data are in general in good agreement. However, for the last three days when the mass concentrations of organics were low, the agreement was poor. The poor agreement may be originated from low organic mass concentrations, which should accompany relatively large uncertainty in the mass spectra. It is suggested from the result in Fig. S10: f_{44} (or H:C) from the online analysis seems sensitive to the subtraction of the contribution of CO_2 in air from the signal at m/z 44 or that of the fragment CO_2^+ when the organic mass concentration was small. Note that the signal at m/z 38 was excluded from the analysis here because $^{38}Ar^+$ from Ar carrier gas presumably influenced it.

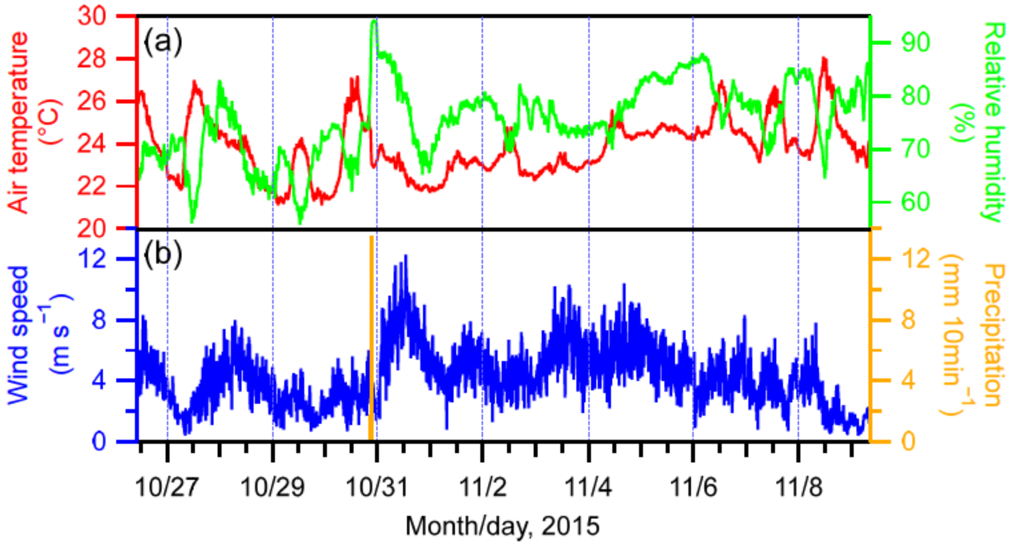

Figure S1: Time series of air temperature (°C), relative humidity (%), wind speed (m s^{-1}), and precipitation (mm 10-min^{-1}) during the sampling period for PM$_{0.95}$.

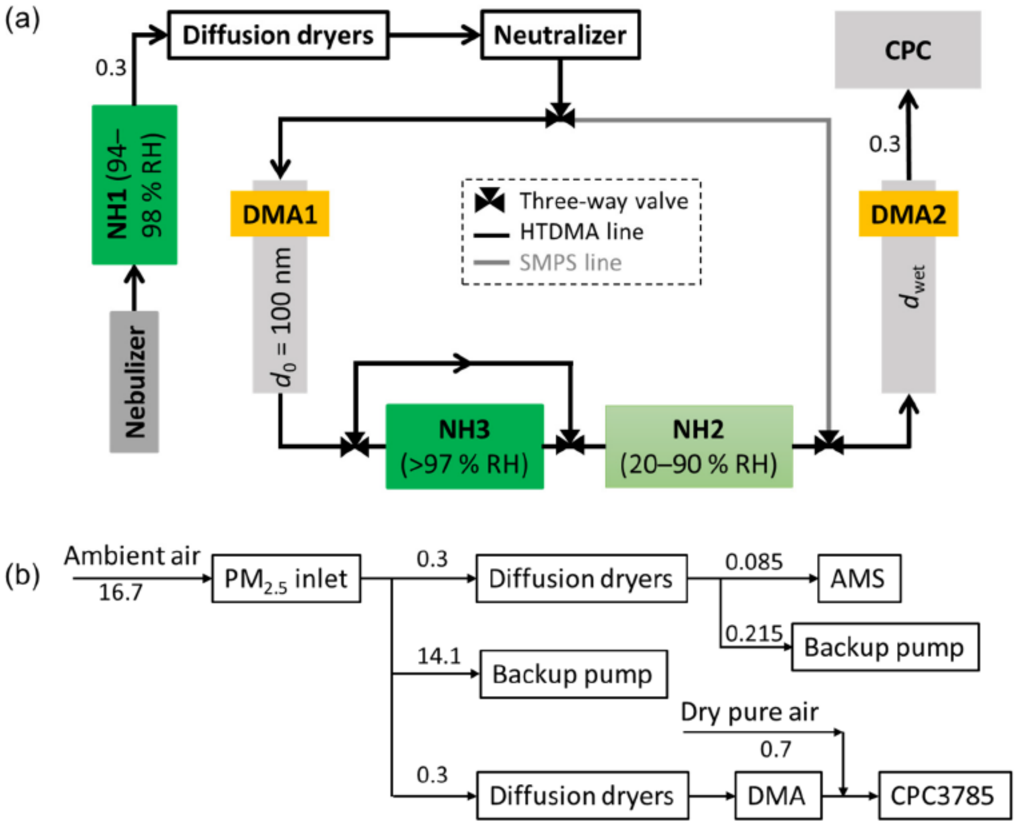

Figure S2: Schematics of the experimental set-up for (a) the offline hygroscopic growth measurements and (b) online AMS/SMPS analyses. Flow rates are in the unit of L min^{-1}. DMA: differential mobility analyzer; CPC: condensation particle counter; NH: Nafion humidifier; AMS: aerosol mass spectrometer.

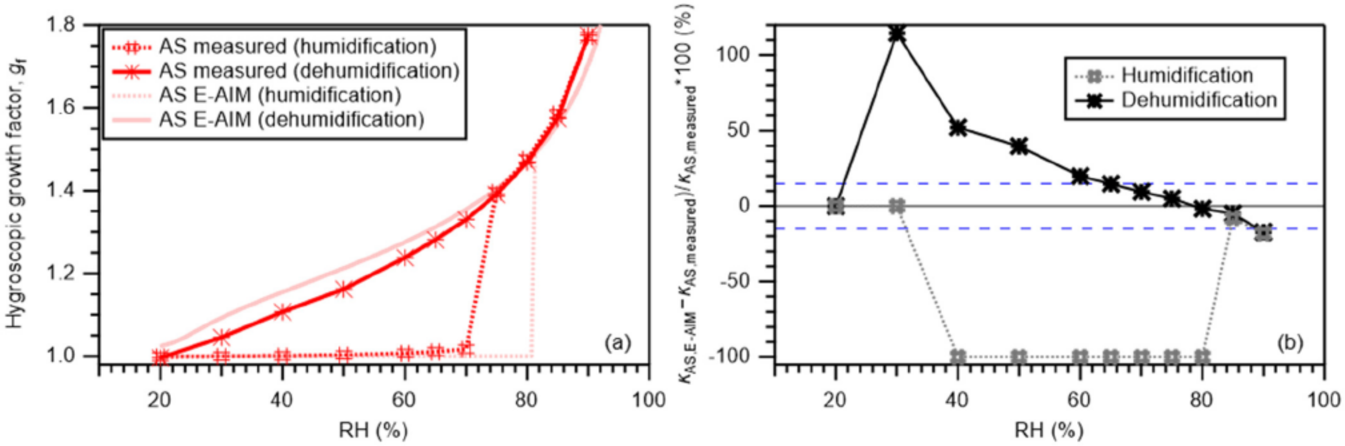

Figure S3: (a) Measured g_f and those predicted based on E-AIM in humidification and dehumidification branches for 100 nm ammonium sulfate (AS) particles. The predicted g_f in the dehumidification branch was obtained based on the assumption that solid salts are not formed. (b) Relative deviation of predicted κ_{AS} ($\kappa_{AS,E\text{-}AIM}$) from measured κ_{AS} ($\kappa_{AS,measured}$) in humidification and dehumidification branches. In both panels, markers represent individual data; lines are used to connect individual data points. The E-AIM predicted results in panel (a) are presented only by lines between points. Blue dashed lines in panel (b) represent +15 % and −15 %.

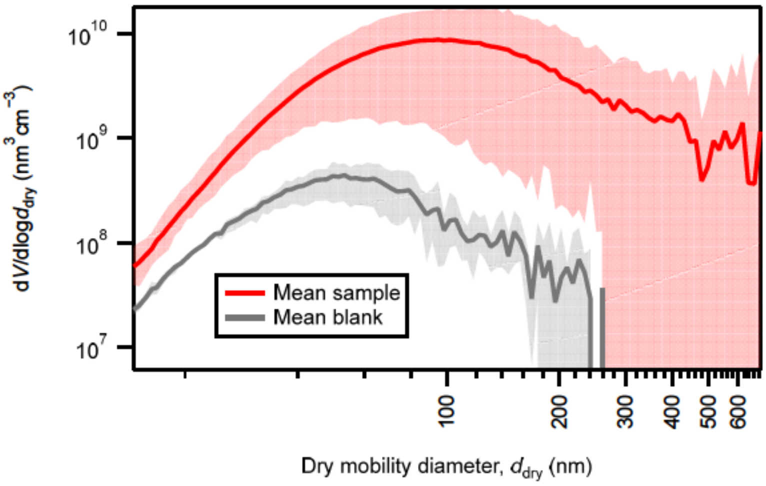

Figure S4: Volume–size distributions of WSM particles generated from ambient aerosol samples and blank samples. The red solid curve and shaded area respectively represent the means and ranges for all ambient aerosol samples. The gray solid curve and shaded area respectively represent the means and ranges of blank samples. Data below the range of the vertical axis are not shown.

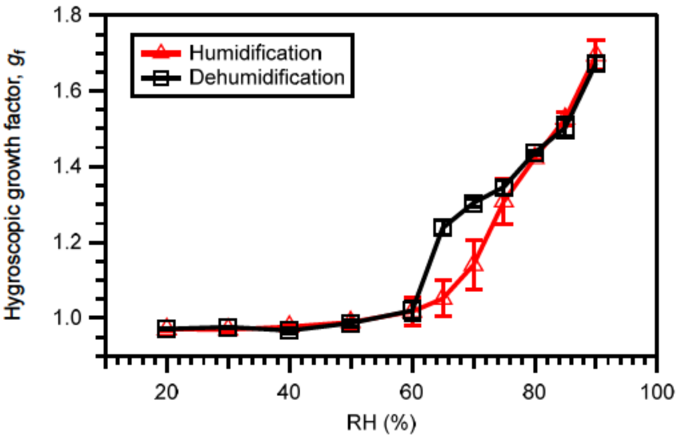

Figure S5: Results representing the repeatability of hygroscopic growth factor measurements: the g_f of 100 nm WSM particles from sample OKNW_035 as a function of RH. Markers and whiskers respectively represent mean values and standard deviations from three measurements (Text S4). The g_f values presented here are not corrected for the slight difference of the sizing (Sect. 2.2) between DMA1 and DMA2.

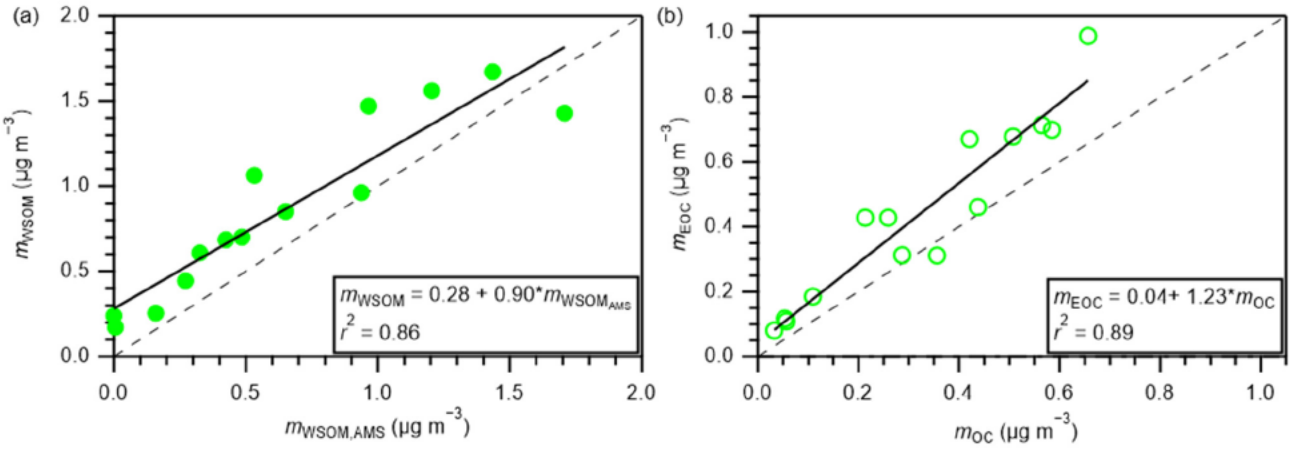

Figure S6: (a) Comparison of the mass concentrations of WSOM derived from WSOC from the TOC analyzer and the AMS-derived OM:OC of WSOM (m_{WSOM}; Sect. 2.3), and those of WSOM from the AMS analysis using phthalic acid as the internal standard ($m_{WSOM,AMS}$; Text S5). (b) Comparison of the mass concentrations of EOC (m_{EOC}) from offline AMS analysis and those of OC (m_{OC}) from the thermal analysis. In both panels, solid and dashed lines respectively represent regression lines and 1:1 lines.

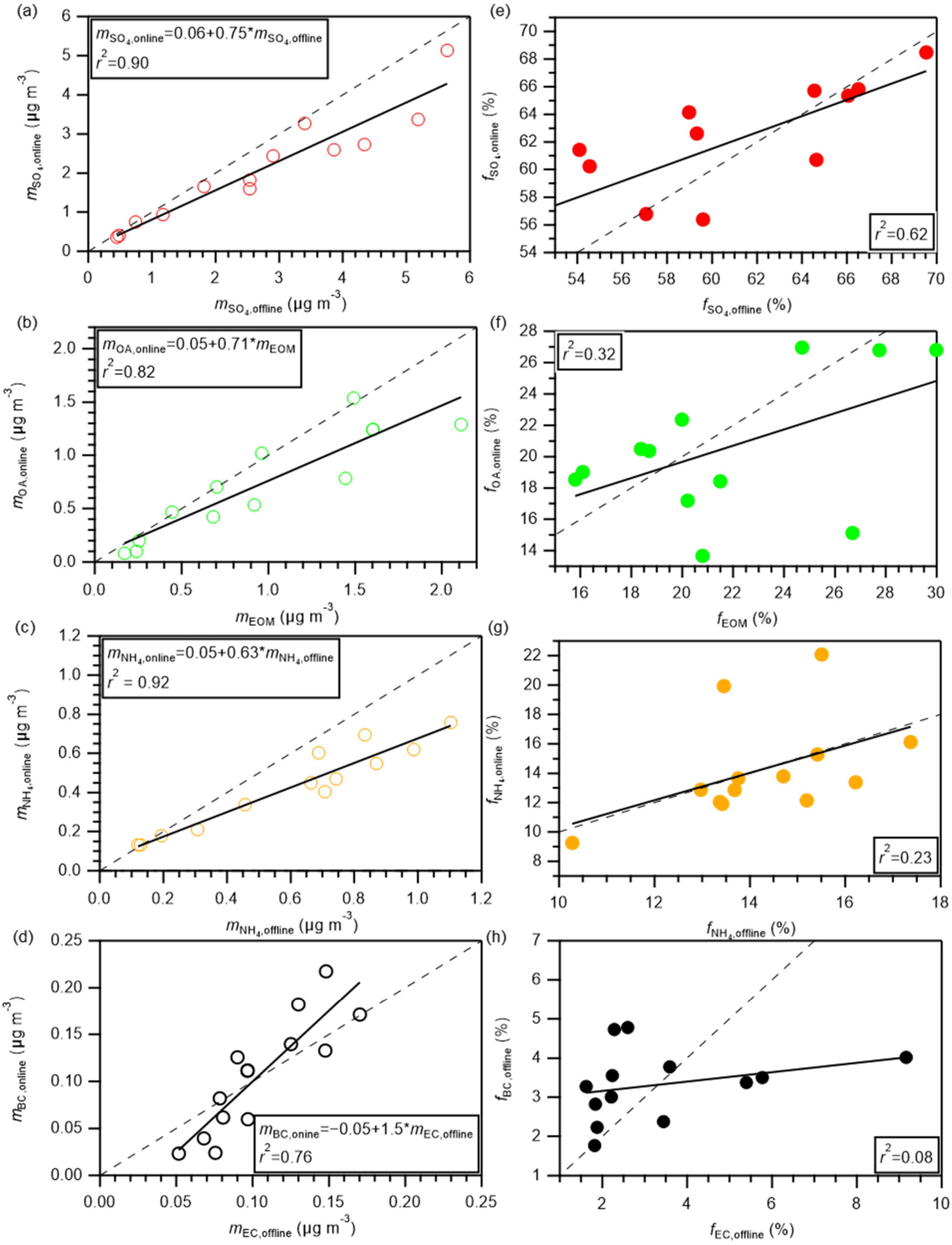

Figure S7: Comparison of the mass concentrations/fractions of chemical components in aerosols obtained from online and offline analyses: (a) mass concentrations of sulfate from online AMS analysis ($m_{SO4,online}$) versus those from offline IC analysis ($m_{SO4,offline}$); (b) mass concentrations of organics from online AMS analysis ($m_{\mathrm{OA,online}}$) and those from offline analysis (m_{EOM}); (c) mass concentrations of ammonium from online AMS analysis ($m_{\mathrm{NH4,online}}$) versus those from offline IC analysis ($m_{\mathrm{NH4,offline}}$); (d) mass concentrations of BC from online COSMOS analysis ($m_{\mathrm{BC,online}}$) versus those from offline thermal analysis ($m_{\mathrm{EC,offline}}$); (e) mass fractions of sulfate in the total mass of SO_4, EOM, NH_4, and BC from online analyses ($f_{\mathrm{SO4,online}}$) versus those in the total mass of SO_4, OA, NH_4, and EC from the offline analyses ($f_{\mathrm{SO4,offline}}$); (f) mass fractions of organics in the total mass of SO_4, EOM, NH_4, and BC from the online analyses ($f_{\mathrm{OA,online}}$) versus those in the total mass of SO_4, OA, NH_4, and EC from offline analyses (f_{EOM}); (g) mass fractions of ammonium in the total mass of SO_4, EOM, NH_4, and BC from online analyses ($f_{\mathrm{NH4,online}}$) versus those in the total mass of SO_4, OA, NH_4, and EC from offline analyses ($f_{\mathrm{NH4,offline}}$); (h) mass fractions of BC in the total mass of SO_4, EOM, NH_4, and BC from online analyses ($f_{\mathrm{BC,online}}$) versus those in the total mass of SO_4, OA, NH_4, and EC from offline analyses ($f_{\mathrm{EC,offline}}$). Solid and dashed lines respectively show regression lines and 1:1 lines.

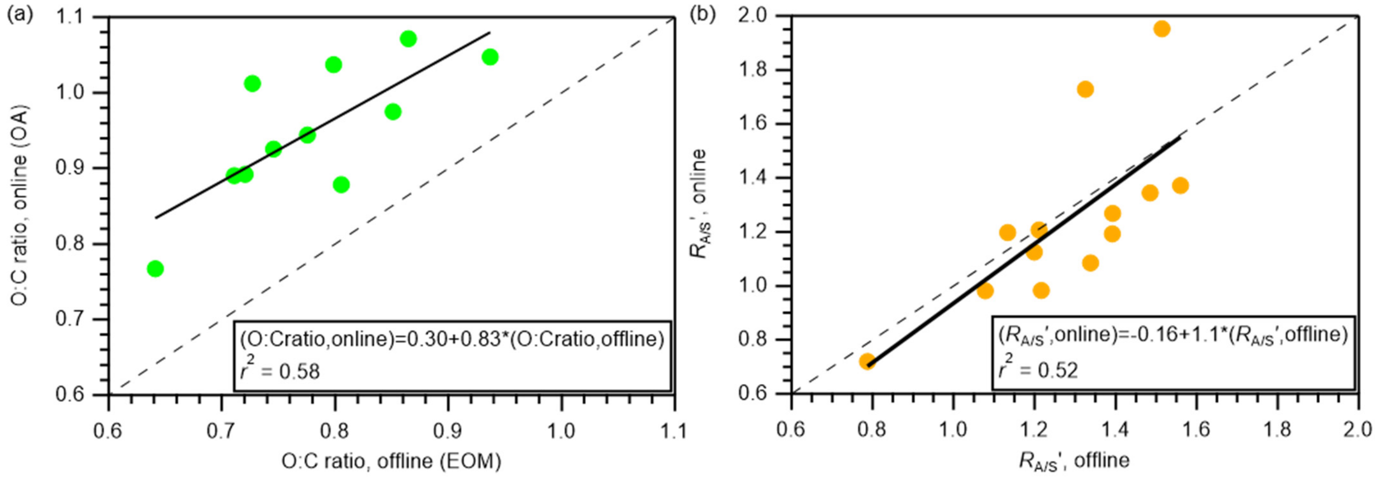

Figure S8: (a) Comparison of the O:C of OA from online analysis to those of EOM from offline analysis. (b) Comparison of the ammonium to sulfate ratio ($R_{A/S}'$) from online and offline analyses (Sect. 3.1). Solid and dashed lines respectively represent regression lines and 1:1 lines.

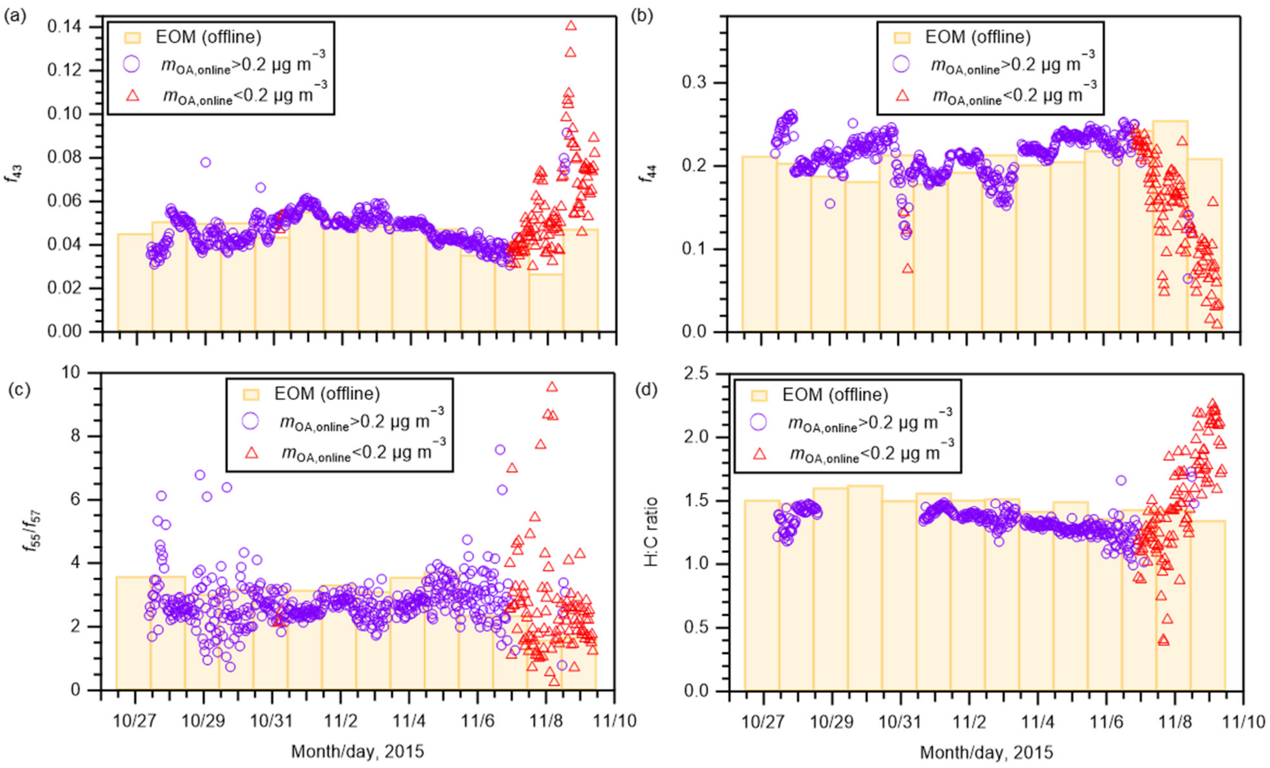

Figure S9: Comparisons between offline and online results of (a) f_{43}, (b) f_{44}, (c) f_{55}/f_{57}, and (d) H:C from the mass spectral analyses for EOM (offline) and organic aerosol (online). Data from offline analysis are presented as bars and those from online analysis for the cases of $m_{\mathrm{OA,online}} > 0.2$ µg m^{-3} and $m_{\mathrm{OA,online}} < 0.2$ µg m^{-3} ($m_{\mathrm{OA,online}}$: mass concentrations of organic aerosol from the online analysis) are presented as open circles and open triangles, respectively. In panel (c), online data with values greater than 10 or smaller than 0 are not presented.

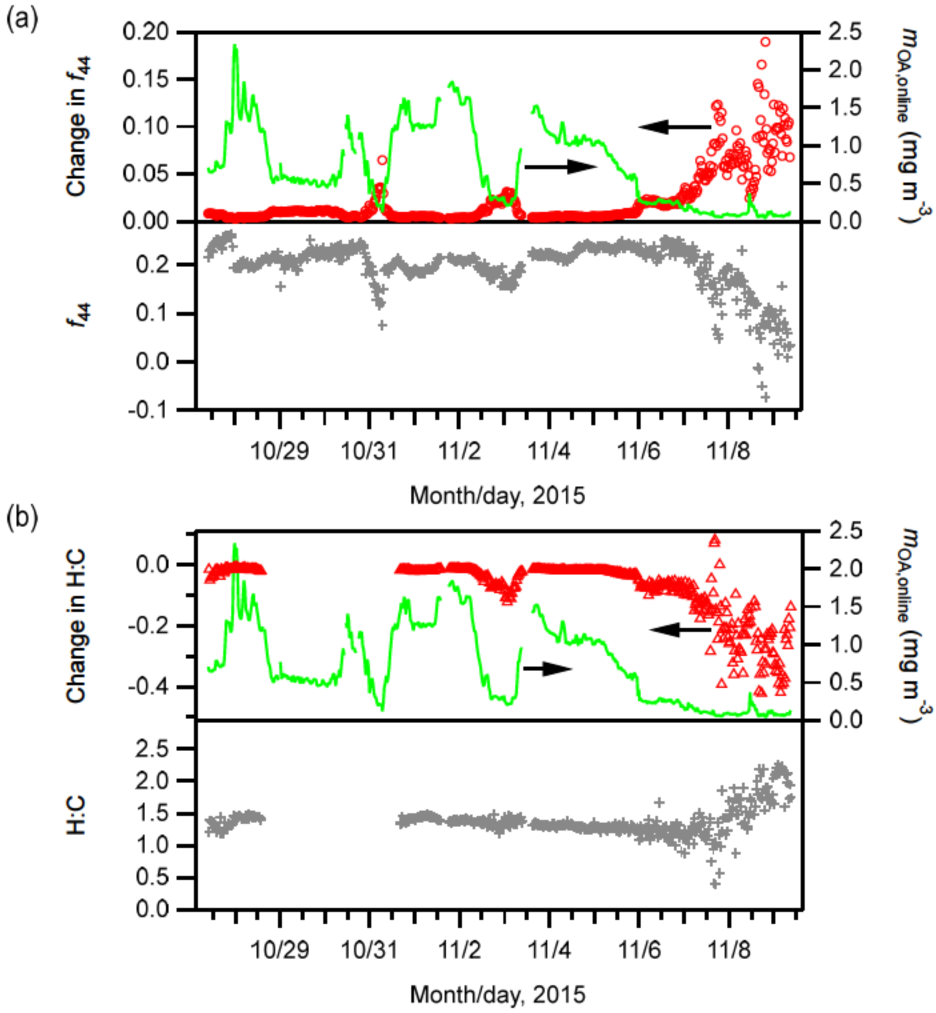

Figure S10: (a) Time series of online f_{44} with fragCO2[44] used for the analyses in this study and the changes in f_{44} (open circles) in the case that 10% lower fragCO2[44] values are used. (b) Time series of online H:C with HR_frag_air[{CO2}] used for the analyses in this study and the changes in H:C (open triangles) in the case that 20% lower HR_frag_air[{CO2}] values are used. The time series of the mass concentrations of organic aerosol from the online analysis ($m_{OA,online}$, green lines) are also shown in both panels.

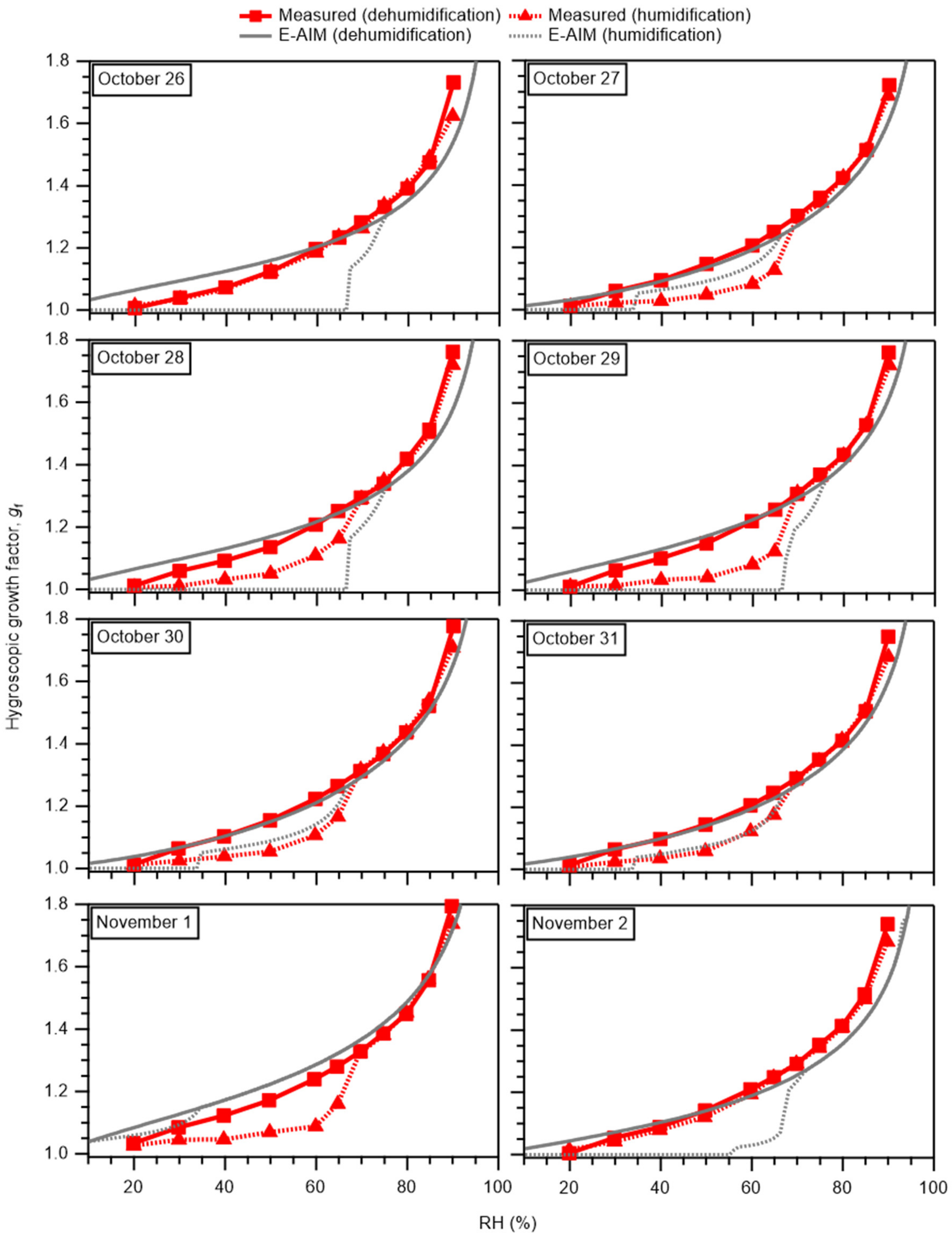

Figure S11: The g_f of 100 nm WSM particles in humidification and dehumidification branches as a function of RH for individual samples. The g_f predicted from the E-AIM model without considering the water retained by WSOM are also presented. Dates shown on panels represent dates when sampling started.

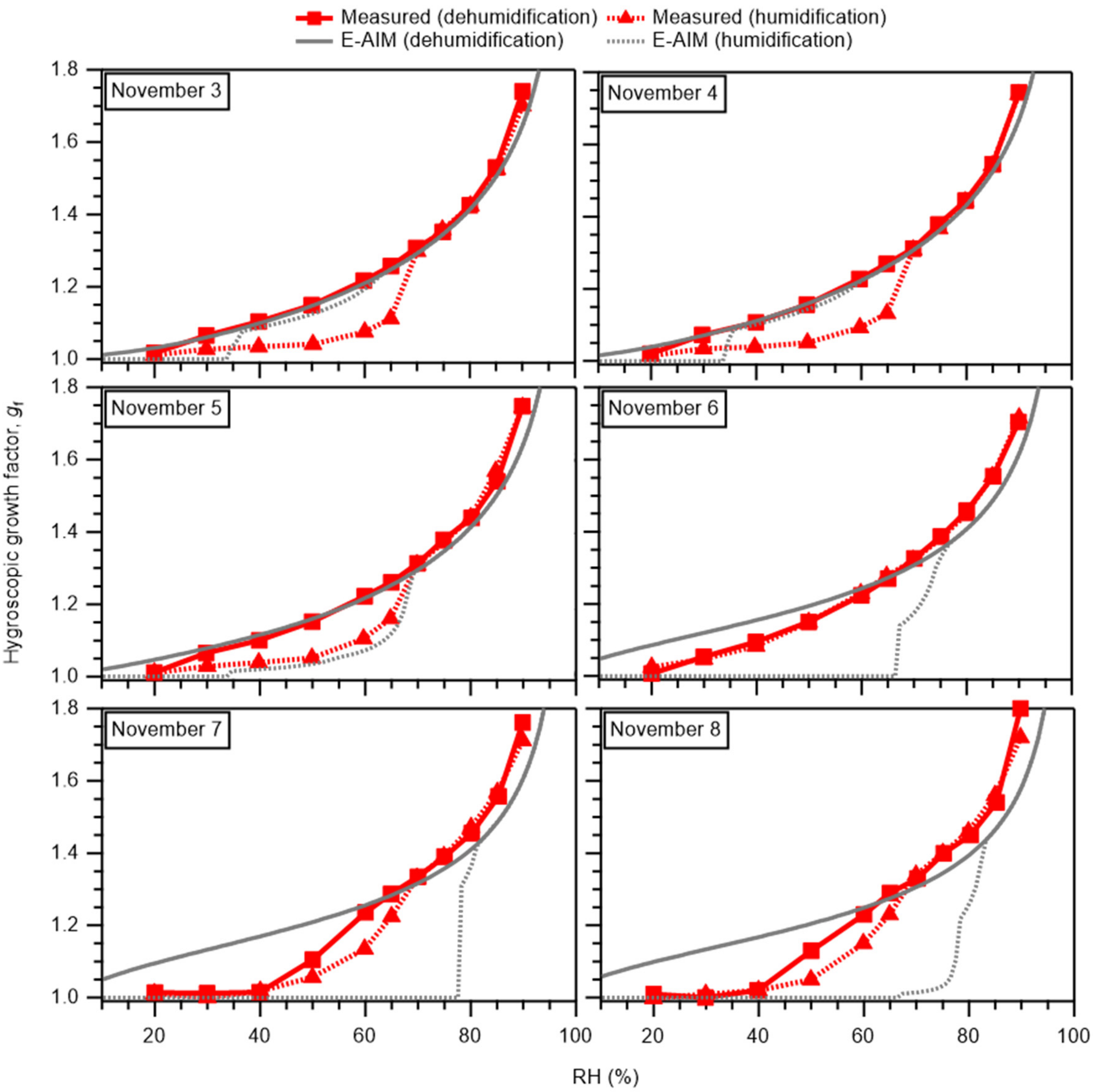

Figure S11 (continued)

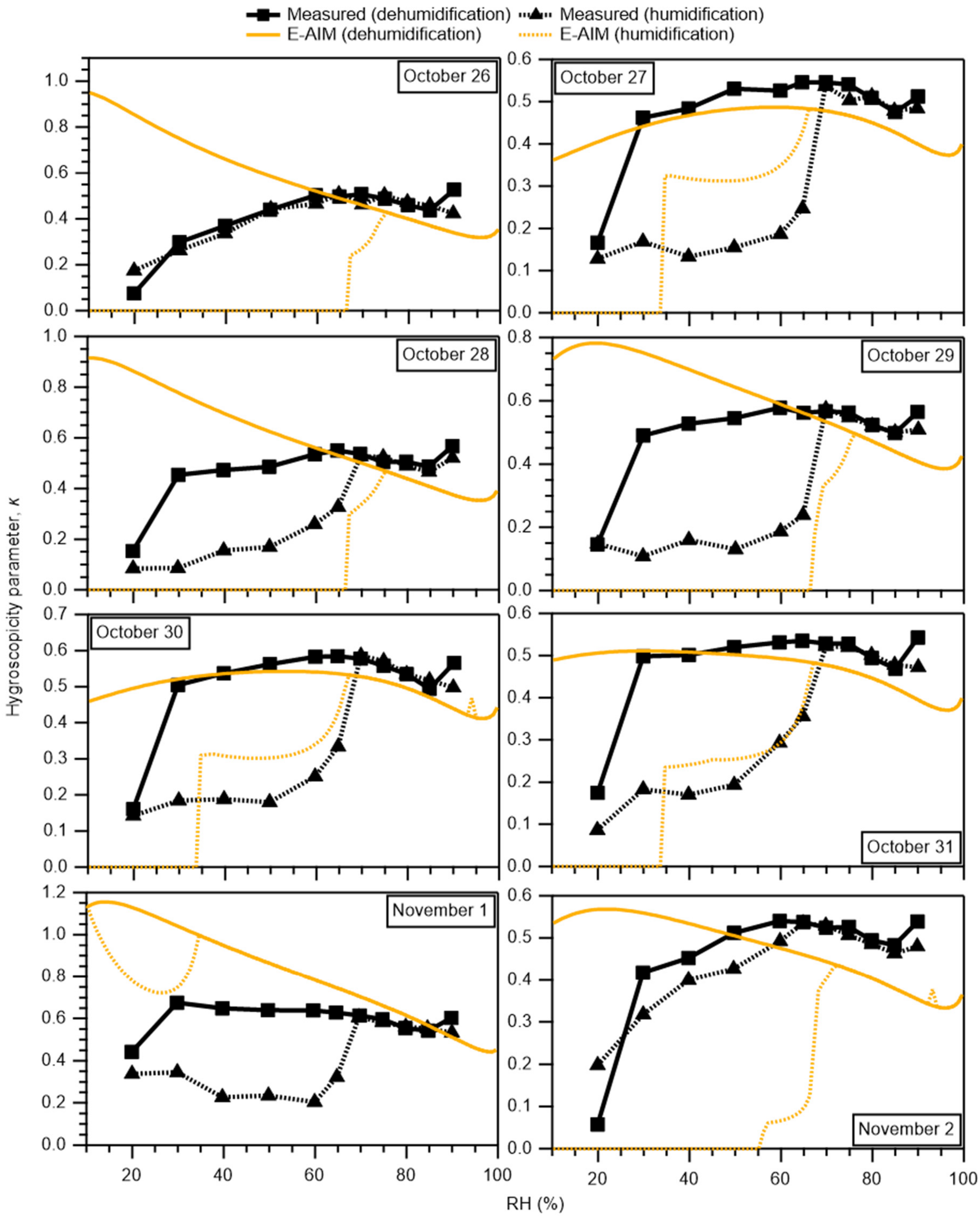

Figure S12: The κ_{WSM} of 100 nm WSM particles in humidification and dehumidification branches as a function of RH. The κ_{WSM} values predicted from the E-AIM model without consideration of water retained by WSOM are also shown. Dates shown on panels represent dates when sampling started.

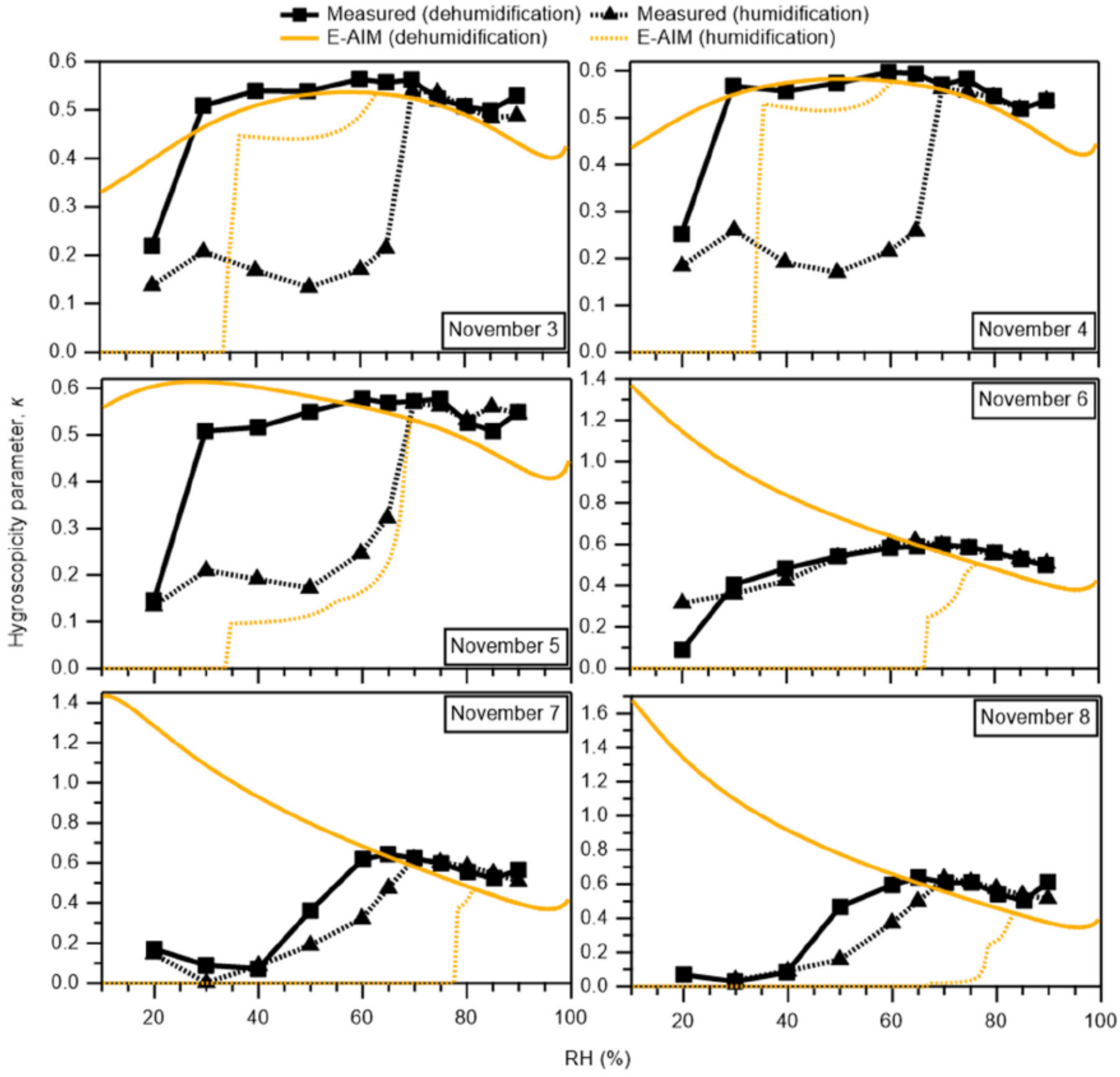

Figure S12 (continued)

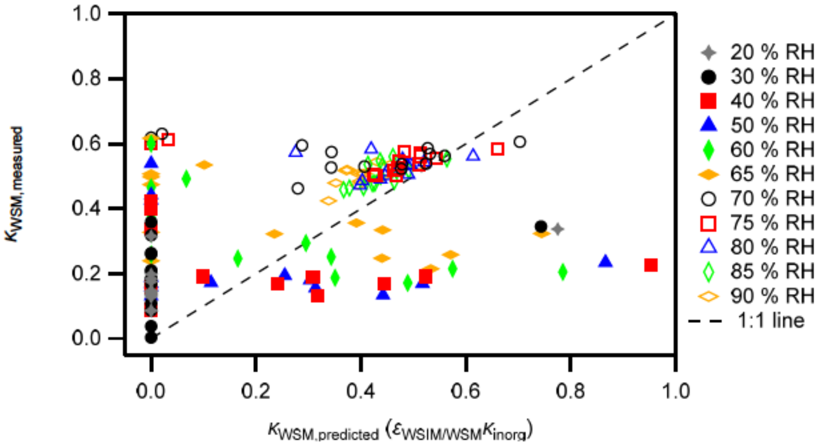

Figure S13: Measured versus predicted κ_{WSM} at different RH in the humidification branch. The dashed line is the 1:1 line.

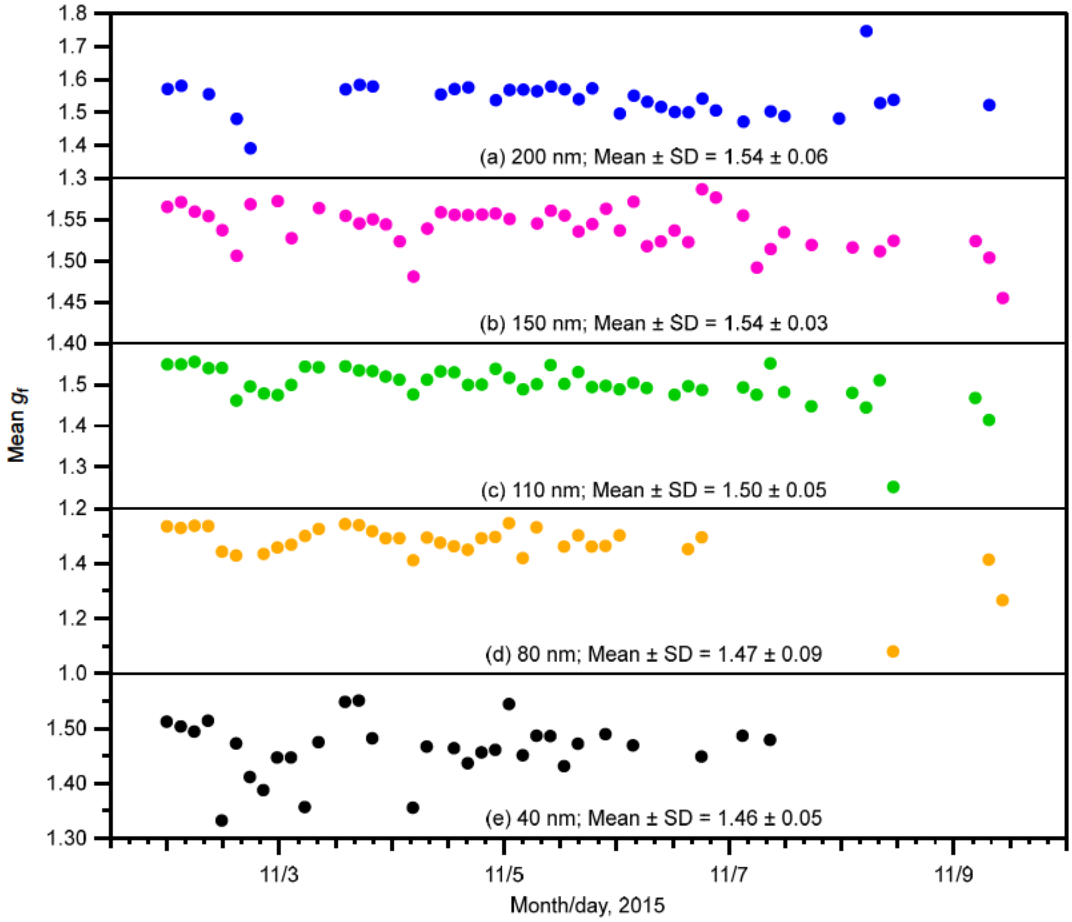

Figure S14: Time series of mean g_f for aerosol particles with different dry diameters. The mean ± SD values for the entire observation period are also presented.

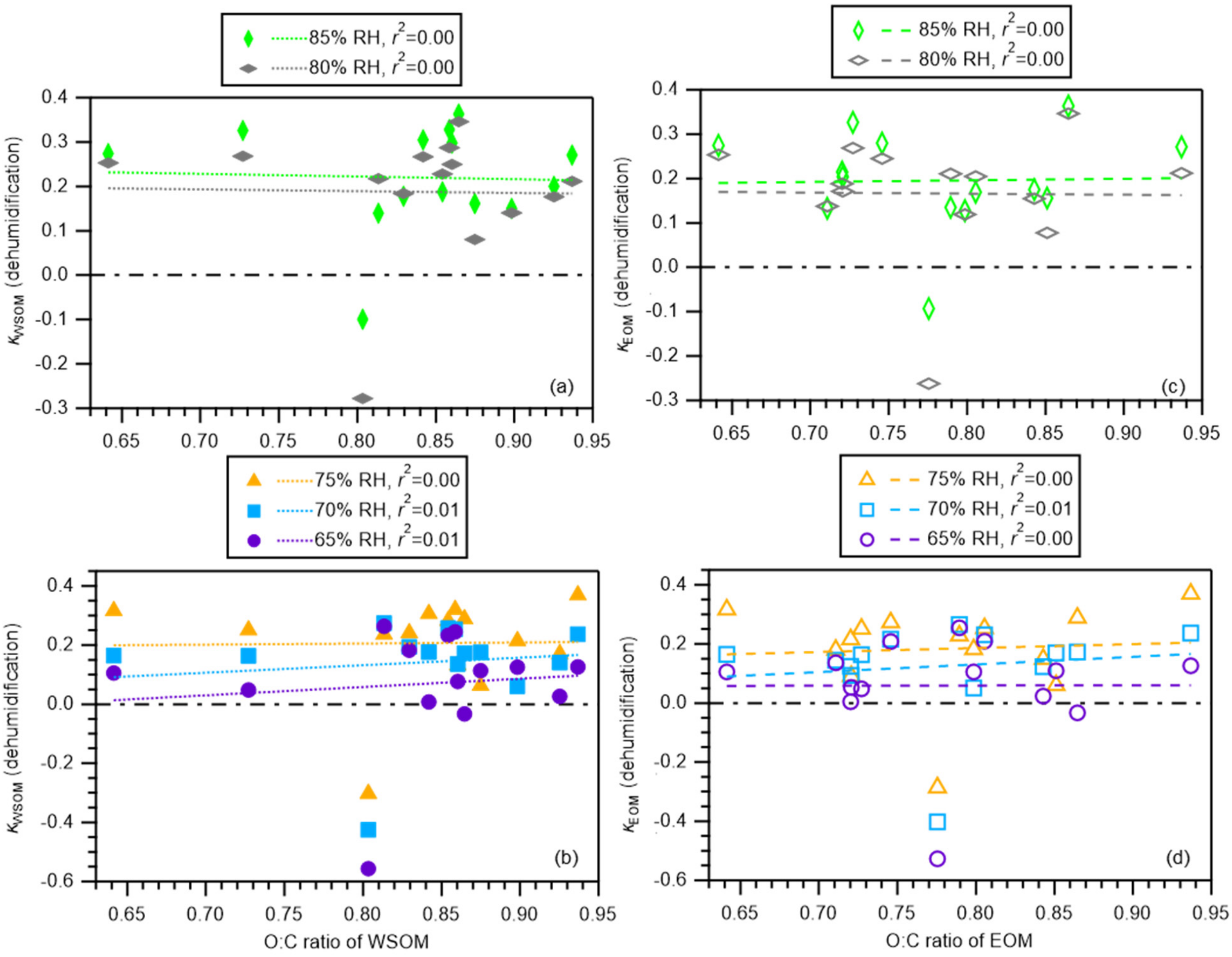

Figure S15: (a and b) Scatter plots of κ_{WSOM} in the dehumidification branch versus O:C of WSOM at (a) 80 and 85 % RH and at (b) 65, 70, and 75 % RH. (c and d) Scatter plots of κ_{EOM} in the dehumidification branch versus O:C of EOM at (c) 80 and 85 % RH and at (d) 65, 70, and 75 % RH.

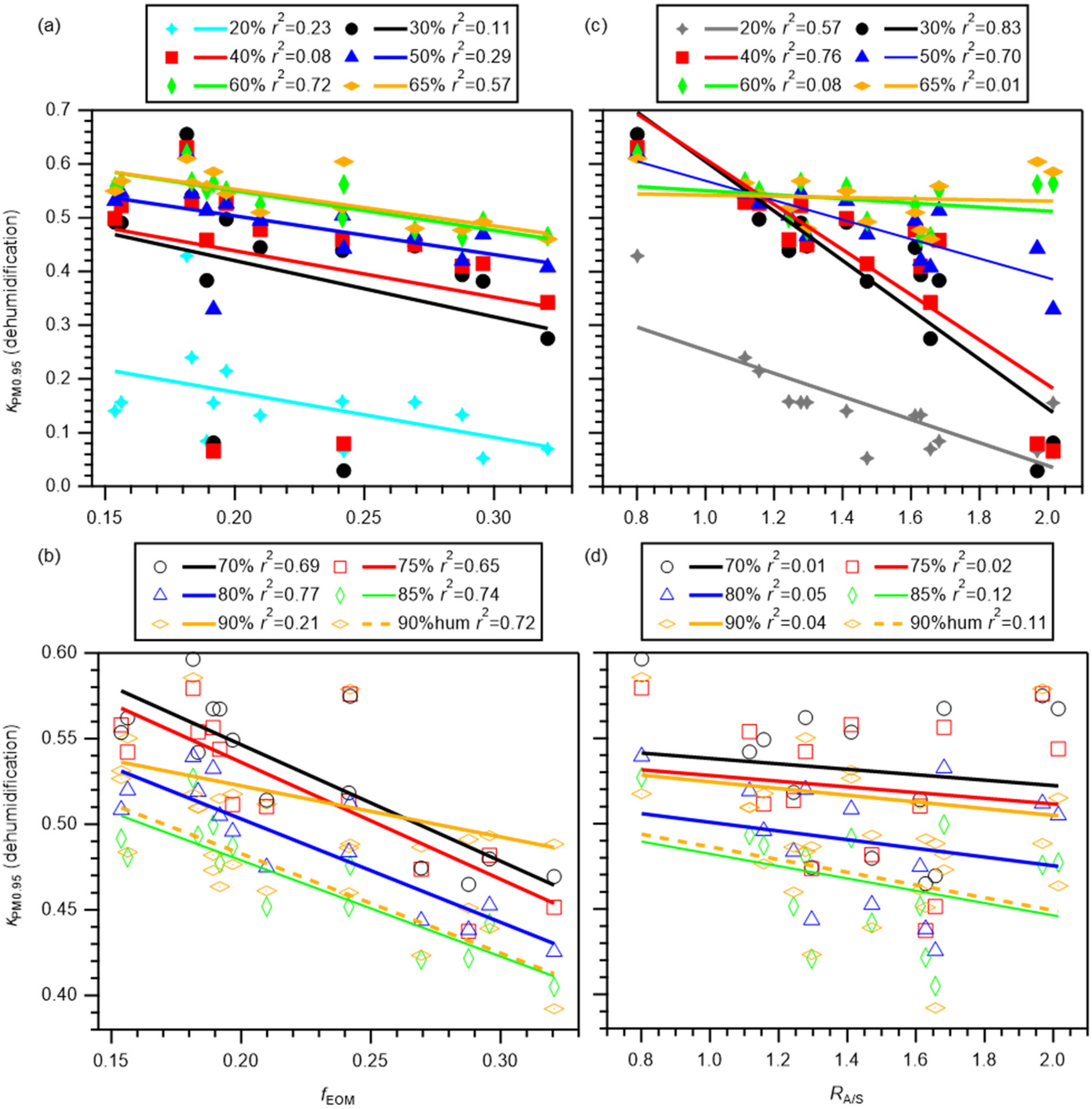

Figure S16: The $\kappa_{\mathrm{PM0.95}}$ values in the dehumidification branch versus (a and b) mass fractions of EOM in PM0.95 (f_{EOM}) and (c and d) the ammonium-to-remaining sulfate molar ratio ($R_{\mathrm{A/S}}$) from offline analysis. Panels a and c present results obtained for 20, 30, 40, 50, 60, and 65 % RH. Panels c and d present results obtained for 70, 75, 80, 85, and 90% RH. The $\kappa_{\mathrm{PM0.95}}$ at 90 % RH in the humidification branch (90%hum) was also compared to (b) f_{WSOM} and (d) $R_{\mathrm{A/S}}$. Coefficients of determination r^2 are also presented.

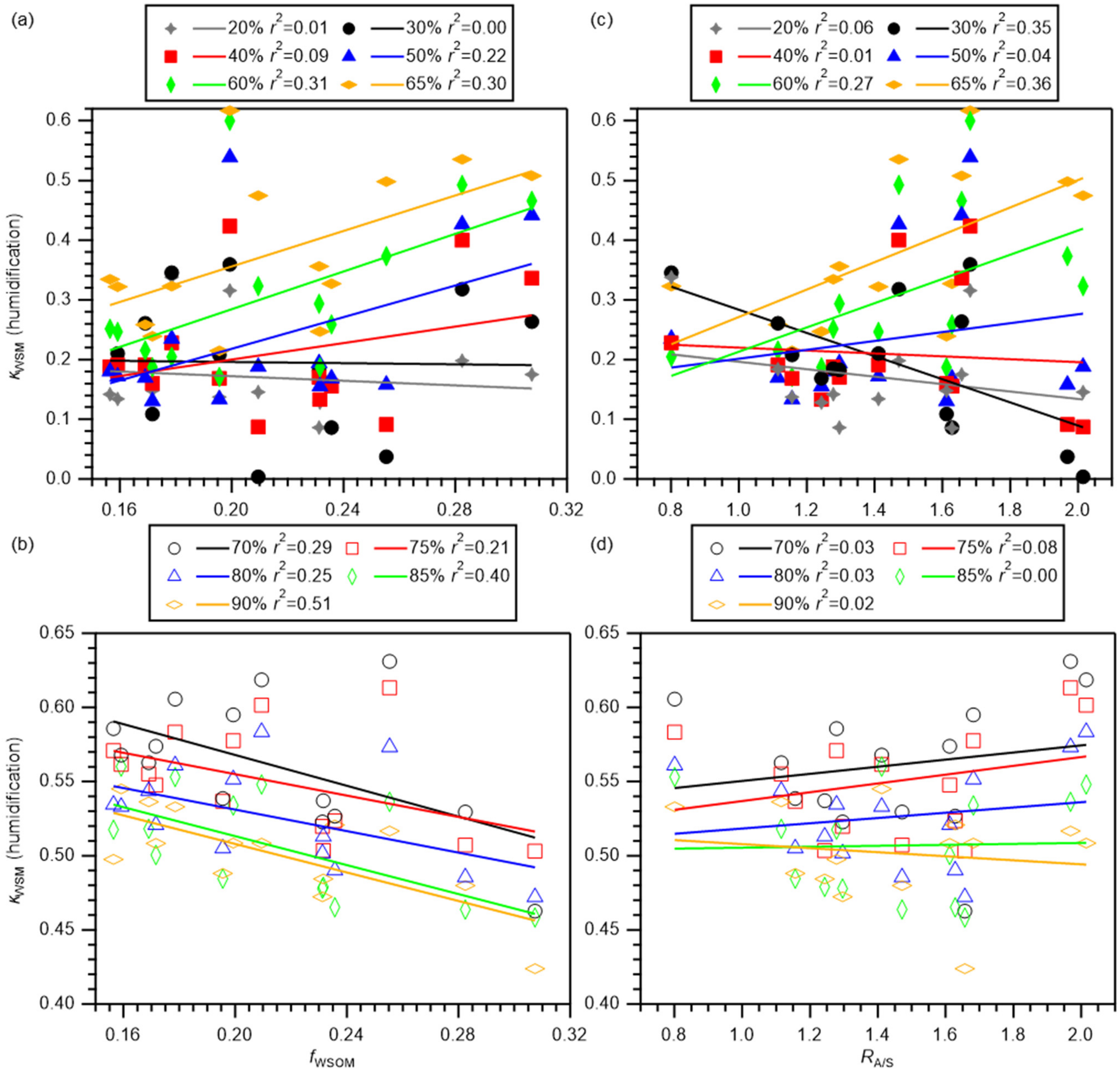

Figure S17: The κ_{WSM} values in the humidification branch versus (a and b) mass fractions of WSOM in WSM (f_{WSOM}) and (c and d) the ammonium-to-remaining sulfate molar ratio ($R_{\mathrm{A/S}}$) from offline analysis. Panels a and c present results obtained for 20, 30, 40, 50, 60, and 65 % RH. Panels c and d present results obtained for 70, 75, 80, 85, and 90 % RH. Coefficients of determination r^2 are also shown.

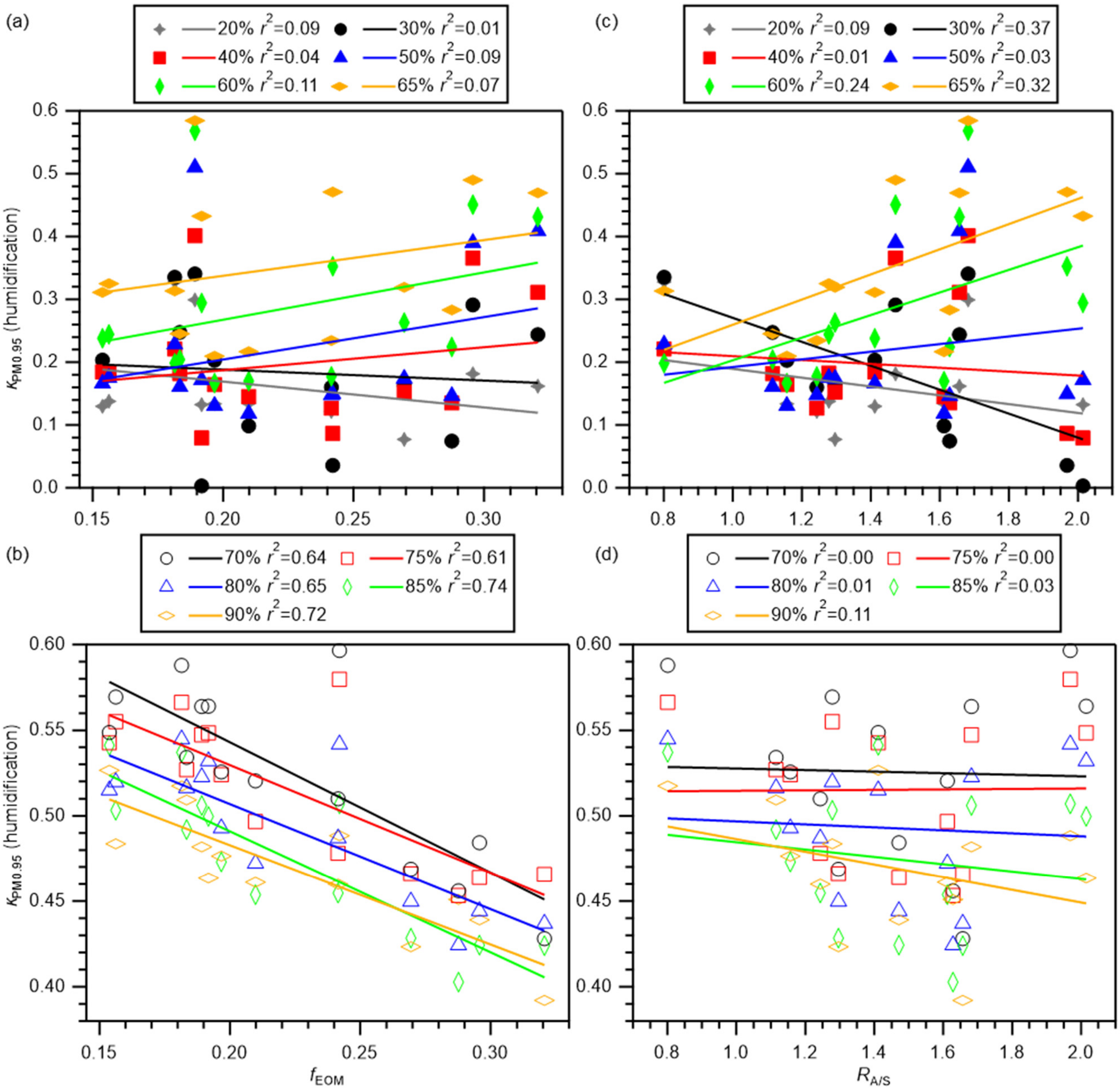

Figure S18: The $\kappa_{PM0.95}$ values in the humidification branch versus (a and b) the mass fractions of EOM in $PM_{0.95}$ (f_{EOM}) and (c and d) the ammonium-to-remaining sulfate molar ratio ($R_{A/S}$) from offline analysis. Panels a and c present results obtained for 20, 30, 40, 50, 60, and 65 % RH. Panels c and d present results obtained for 70, 75, 80, 85, and 90 % RH. Coefficients of determination r^2 are also presented.

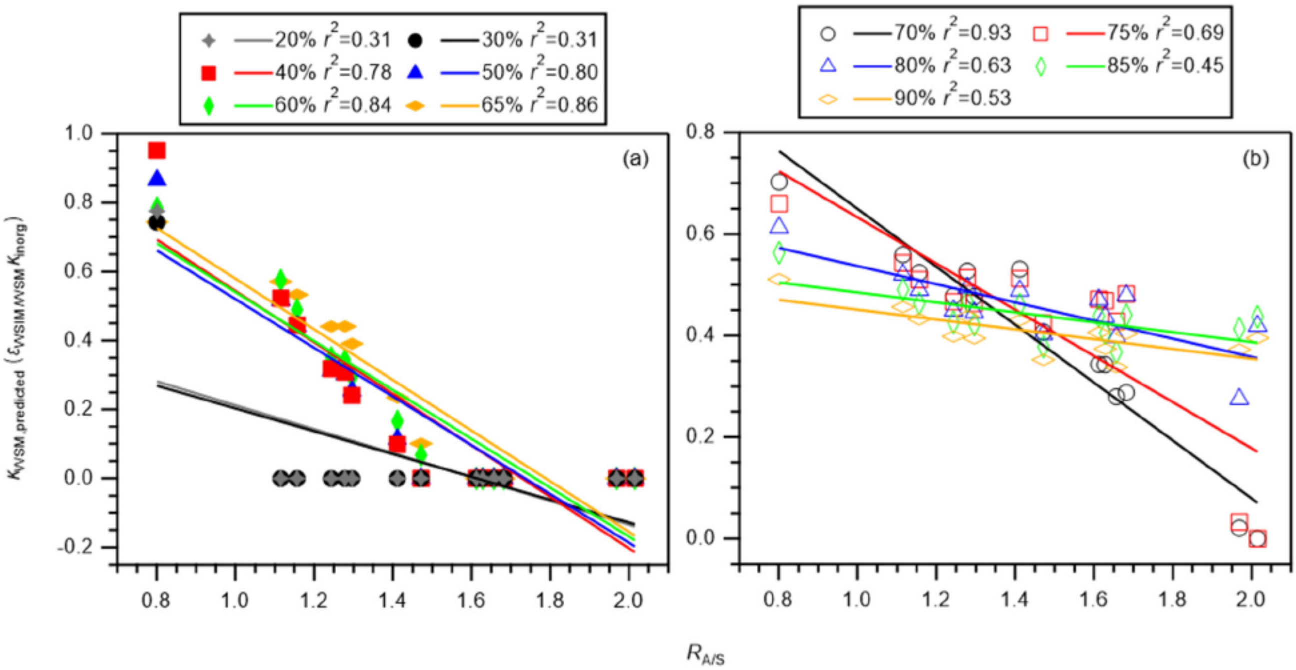

Figure S19: Scatter plots of predicted κ_{WSM} versus $R_{\mathrm{A/S}}$ of WSM at (a) 20, 30, 40, 50, 60, and 65 % RH and (b) 70, 75, 80, 80, and 90 % RH. Markers and lines respectively represent individual data and regression lines. Coefficients of determination are also presented.

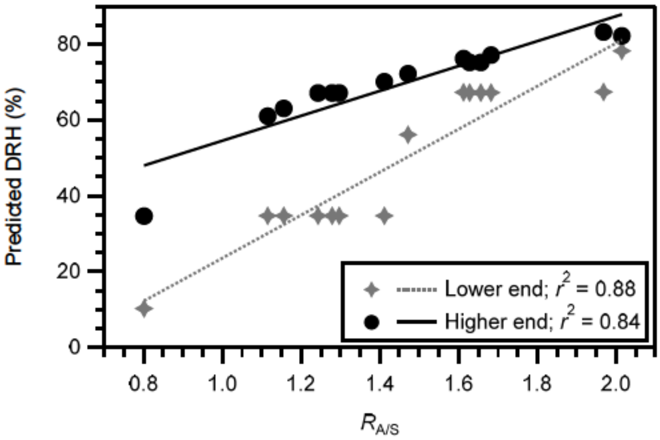

Figure S20: Scatter plots of DRH predicted by E-AIM versus $R_{\mathrm{A/S}}$ of WSM. Gray stars present the predicted RH at which the g_{f} in the humidification branch became greater than unity (lower end), and the dotted line represents the corresponding regression line. Black circles show the predicted RH at which the g_{f} in the humidification and dehumidification branches became identical (higher end), and the solid line represents the corresponding regression line.

Table S1: Sampling periods and sampled air volumes for the $PM_{0.95}$ studied

Sample ID	Period (in 2015, JST)	Air volume (m^3)
OKNW_001	26 Oct, 09:56:00 – 27 Oct, 09:00:03	1569.5
OKNW_003	27 Oct, 09:26:00 – 28 Oct, 09:00:00	1602.9
OKNW_005B*	28 Oct, 09:11:11 – 28 Oct, 09:11:21	0
OKNW_006	28 Oct, 09:43:30 – 29 Oct, 09:00:00	1584.5
OKNW_009	29 Oct, 09:24:00 – 30 Oct, 09:00:00	1608.7
OKNW_011	30 Oct, 09:23:00 – 31 Oct, 09:00:00	1612.5
OKNW_014	31 Oct, 09:46:00 – 1 Nov, 09:00:00	1588.1
OKNW_017	1 Nov, 09:34:10 – 2 Nov, 09:00:01	1602.8
OKNW_019B*	2 Nov, 09:39:00 – 2 Nov, 09:39:10	0
OKNW_020	2 Nov, 09:59:45 – 3 Nov, 09:00:00	1574.7
OKNW_023	3 Nov, 09:20:00 – 4 Nov, 09:00:00	1621.2
OKNW_025	4 Nov, 09:22:40 – 5 Nov, 09:00:00	1619.9
OKNW_028	5 Nov, 09:44:40 – 6 Nov, 09:00:00	1595.9
OKNW_045B*	6 Nov, 09:19:20 – 6 Nov, 09:19:30	0
OKNW_032	6 Nov, 09:49:30 – 7 Nov, 09:00:00	1590.7
OKNW_035	7 Nov, 09:24:40 – 8 Nov, 09:00:02	1619.8
OKNW_037	8 Nov, 09:25:00 – 9 Nov, 09:00:00	1620.2
OKNW_039B*	9 Nov, 09:16:00 – 9 Nov, 09:16:10	0

* Field blanks

Table S2: Mode diameters of PSL size standards measured using DMA1, DMA2, and SMPS (in nm)[a]

Manufacturer's warranty[b]	**HTDMA**		**Online SMPS**
	DMA1	**DMA2**	
55 (± 1)	-	61.8 ± 0.3	60.3 ± 0.2
100 (± 3)	100.8 ± 0.0	103.2 ± 0.2	102.8 ± 0.3
309 (± 9)	303.3 ± 0.2	314.8 ± 1.1	307.5 ± 0.2 (308.4 ± 0.3)
498 (± 9)	-	516.7 ± 1.2	503.4 ± 0.5

[a] The mean ± SD of the mode diameters from fittings. Results are based on calibrations done before analysis of atmospheric samples, except for the case of 309 nm PSL size standards from the SMPS, for which calibration was also made after sample analysis (in parenthesis).

[b] Mean diameter (± expanded uncertainty; *k* = 2).

Table S3: Mass concentrations of water-soluble ions (μg m^{-3}) and water-soluble organic carbon (WSOC, μgC m^{-3}) in $PM_{0.95}$[a]

Sample ID	MSA	Cl^-	NO_3^-	SO_4^{2-}	NH_4^+	Na^+	K^+	Ca^{2+}	Mg^{2+}	WSOC
OKNW_001	0.0107	BDL	0.0033	1.5761	0.4333	0.0877	0.045	0.0079	0.0118	0.4022
OKNW_003	0.0316	BDL	0.0035	3.8618	0.8696	0.0656	0.0594	0.0105	0.0099	0.6412
OKNW_006	0.025	0.0017	0.0063	2.5378	0.7076	0.1069	0.0519	0.0224	0.0147	0.4613
OKNW_009	0.0157	BDL	0.0025	2.5371	0.743	0.0396	0.0418	0.0126	0.0053	0.3079
OKNW_011	0.0154	BDL	0.0015	2.9046	0.6634	0.0677	0.0415	0.0087	0.0089	0.3015
OKNW_014	0.0413	0.0012	0.0091	4.3392	0.9866	0.1371	0.0482	0.0124	0.0194	0.7385
OKNW_017	0.0425	BDL	0.0052	5.6403	0.8334	0.0475	0.0327	0.0068	0.0091	0.6412
OKNW_020	0.0098	0.0016	0.0043	1.1744	0.3069	0.0306	0.0152	0.0063	0.0049	0.2646
OKNW_023	0.0399	0.0006	0.0054	5.1817	1.1029	0.0483	0.0592	0.0063	0.0068	0.673
OKNW_025	0.0249	BDL	0.0019	3.3991	0.6882	0.0536	0.0301	0.0057	0.0077	0.3632
OKNW_028	0.0209	BDL	0.0017	1.8159	0.4562	0.0453	0.0165	0.0059	0.0055	0.1845
OKNW_032	0.0109	BDL	0.0008	0.7429	0.1942	0.0613	0.0108	0.0053	0.0074	0.1091
OKNW_035	0.0054	BDL	0.0006	0.4499	0.1279	0.0535	0.0056	0.0044	0.0054	0.0796
OKNW_037	0.0074	0.0006	0.0018	0.4839	0.1204	0.0757	0.0042	0.0047	0.0051	0.1169
Mean	0.0215	0.0059	0.0034	2.6175	0.5881	0.0657	0.0330	0.0086	0.0087	0.3775

[a] Data were corrected for field blanks. BDL, below detection limit (i.e., mean + three times standard deviation of blank samples).

Table S4: Summary of offline measurements

Instrument	Observed component/property
HTDMA	g_f of WSM at 20, 30, 40, 50, 60, 65, 70, 75, 80, 85, and 90 RH in humidification and dehumidification branches
IC	SO_4^{2-}, NO_3^-, Cl^-, NH_4^+, Na^+, K^+, Ca^{2+}, Mg^{2+}, and MSA
TOC	WSOC and WSOM (also from AMS-derived OM:OC)
AMS	O:C, H:C, OM:OC, densities of WSOM and WISOM, WISOM, EOM, WISOC, and EOC
Carbon analyzer	OC and EC

Table S5: Mean ± standard deviation of g_f, κ_{WSM}, $\kappa_{PM0.95}$, κ_{WSOM}, and κ_{EOM} in humidification and dehumidification branches

RH (%)	Humidification					Dehumidification				
	g_f	κ_{WSM}	$\kappa_{PM0.95}$	κ_{WSOM}	κ_{EOM}	g_f	κ_{WSM}	$\kappa_{PM0.95}$	κ_{WSOM}	κ_{EOM}
20	1.01±0.01	0.17±0.08	0.16±0.07	-	-	1.01±0.01	0.17±0.10	0.16±0.10	-	-
30	1.03±0.01	0.20±0.11	0.18±0.10	-	-	1.05±0.02	0.42±0.18	0.40±0.17	-	-
40	1.04±0.02	0.21±0.10	0.20±0.10	-	-	1.09±0.03	0.45±0.17	0.42±0.16	-	-
50	1.07±0.04	0.24±0.13	0.22±0.12	-	-	1.14±0.02	0.52±0.07	0.49±0.07	-	-
60	1.13±0.05	0.30±0.13	0.28±0.12	-	-	1.22±0.01	0.57±0.04	0.53±0.05	-	-
65	1.18±0.05	0.38±0.13	0.35±0.12	-	-	1.26±0.02	0.57±0.04	0.54±0.05	0.07±0.20	0.06±0.19
70	1.31±0.02	0.56±0.05	0.53±0.05	-	-	1.31±0.02	0.57±0.04	0.53±0.04	0.14±0.17	0.13±0.16
75	1.36±0.02	0.55±0.04	0.52±0.04	-	-	1.37±0.02	0.56±0.04	0.52±0.05	0.21±0.17	0.18±0.16
80	1.43±0.02	0.53±0.03	0.49±0.04	-	-	1.43±0.02	0.52±0.03	0.49±0.04	0.19±0.15	0.17±0.14
85	1.53±0.03	0.51±0.04	0.47±0.04	0.26±0.15	0.24±0.16	1.53±0.02	0.50±0.03	0.47±0.03	0.22±0.12	0.20±0.11
90	1.71±0.03	0.50±0.03	0.47±0.04	-	-	1.75±0.03	0.55±0.03	0.52±0.03	-	-

Table S6: Fractional contribution of WSOM to the κ values of WSM and $PM_{0.95}$ (mean ± standard deviation, %)

RH (%)	Humidification		Dehumidification	
	$(\varepsilon_{WSOM/WSM} \times \kappa_{WSOM})/\kappa_{WSM} \times 100$	$(\varepsilon_{WSOM/PM0.95} \times \kappa_{WSOM})/\kappa_{PM0.95} \times 100$	$(\varepsilon_{WSOM/WSM} \times \kappa_{WSOM})/\kappa_{WSM} \times 100$	$(\varepsilon_{WSOM/PM0.95} \times \kappa_{WSOM})/\kappa_{PM0.95} \times 100$
65	-	-	4±8	4±8
70	-	-	7±7	7±7
75	-	-	10±7	10±7
80	-	-	10±7	10±7
85	13±7	13±7	12±7	12±7

References

Chen, Q., Ikemori, F., Nakamura, Y., Vodicka, P., Kawamura, K., and Mochida, M.: Structural and light-absorption characteristics of complex water-insoluble organic mixtures in urban submicrometer aerosols, Environmental Science & Technology, 51, 8293-8303, 10.1021/acs.est.7b01630, 2017.

Han, Y. M., Kawamura, K., Chen, Q. C., and Mochida, M.: Formation of high-molecular-weight compounds via the heterogeneous reactions of gaseous C-8-C-10 n-aldehydes in the presence of atmospheric aerosol components, Atmospheric Environment, 126, 290-297, 10.1016/j.atmosenv.2015.11.050, 2016.

Jung, J. S., Kim, Y. J., Aggarwal, S. G., and Kawamura, K.: Hygroscopic property of water-soluble organic-enriched aerosols in Ulaanbaatar, Mongolia during the cold winter of 2007, Atmospheric Environment, 45, 2722-2729, 10.1016/j.atmosenv.2011.02.055, 2011.

Park, K., Kittelson, D. B., Zachariah, M. R., and McMurry, P. H.: Measurement of inherent material density of nanoparticle agglomerates, J. Nanopart. Res., 6, 267-272, 10.1023/B:NANO.0000034657.71309.e6, 2004.

Petters, M. D., and Kreidenweis, S. M.: A single parameter representation of hygroscopic growth and cloud condensation nucleus activity, Atmospheric Chemistry and Physics, 7, 1961-1971, 10.5194/acp-7-1961-2007, 2007.

Tang, I. N., and Munkelwitz, H. R.: Water Activities, Densities, and Refractive-Indexes of Aqueous Sulfates and Sodium-Nitrate Droplets of Atmospheric Importance, Journal of Geophysical Research-Atmospheres, 99, 18801-18808, 10.1029/94jd01345, 1994.